

**A Multi-Resonance Thermally Activated Delayed Fluorescence Emitter with a
Twisted Second-Generation Carbazole Dendron Showing Suppressed
Concentration Quenching and Its Use in Solution-Processed Organic Light-
Emitting Diodes**

*Jingxiang Wang^a, Yuka Yasuda^b, Yongxia Ren^b, Ryo Kondo^b, David B. Cordes^a,
Hironori Kaji^{b*} and Eli Zysman-Colman^{a*}*

^a Organic Semiconductor Centre, EaStCHEM School of Chemistry, University of St Andrews, St Andrews, Fife, UK, KY16 9ST, Fax: +44-1334 463808; Tel: +44-1334 463826; E-mail: eli.zysman-colman@st-andrews.ac.uk.

^b Institute for Chemical Research, Kyoto University, Uji, Kyoto, 611-0011, Japan, Tel: +81-0774-38-3149; E-mail: kaji@scl.kyoto-u.ac.jp.

Table of Contents

General information.....	S3
Synthesis.....	S7
Computations.....	S27
Photophysical characterization.....	S27
Devices	S30
References	S31

General information:

General synthetic information.

All reagents and solvents for the synthesis and characterization were obtained from commercial sources and used as received. Anhydrous THF and toluene were obtained from an MBraun SPS5 solvent purification system. Other chemicals were used directly without additional purification. Air-sensitive reactions are conducted under a nitrogen atmosphere using Schlenk techniques. Flash column chromatography was carried out using silica gel (Silica-P from Silicycle, 60 Å, 40-63 µm). Analytical thin-layer-chromatography (TLC) was performed with silica plates with plastic backings (250 µm with F-254 indicator). TLC visualization was accomplished by 254 and 365 nm UV lamp. Melting points were measured using open-ended capillaries on an Electrothermal 1101D Mel-Temp apparatus and are uncorrected. HPLC analysis was conducted on a Shimadzu LC-40 HPLC system. HPLC traces were performed using a Shim-pack GIST 3µm C18 reverse phase analytical column. ¹H and ¹³C NMR spectra were measured using a Bruker AVII 400 and Bruker AVIII-HD 500 NMR spectrometers. The following abbreviations have been used for multiplicity assignments: “s” for singlet, “d” for doublet, “dd” for doublet of doublets and “m” for multiplet. High-resolution mass spectrometry (HRMS) was obtained at the University of Edinburgh Mass Spectrometry Facility. Elemental analyses were performed by Joe Casillo at the University of Edinburgh.

Theoretical Calculations.

All ground-state optimizations were carried out using Density Functional Theory (DFT) level with Gaussian 16¹ using the PBE0² functional and the 6-31G(d,p) basis set³, starting from a structure drawn and optimized using Chem3D. Excited-state calculations were performed using Time-Dependent DFT (TD-DFT) within the Tamm-Dancoff approximation (TDA)^{4,5} using the same functional and basis set as for ground state geometry optimization. Molecular orbitals were visualized using GaussView 6.0 software.⁶ Vertical excited states were also calculated using Spin-Component Scaling second-order algebraic diagrammatic construction (SCS-ADC2)/cc-pVDZ calculations based on the ground-state optimized structure using DFT method.^{7,8} The spin-orbit coupling matrix elements were calculated based on the optimized T₁

geometry at the PBE0/6-31G(d,p) level of theory with Gaussian 16¹. Difference density plots were used to visualize change in electronic density between the ground and excited state and were visualized using the VESTA package.⁹ Calculations were submitted and processed using the Digichem software package (version 5),^{10, 11} which incorporates a number of publicly available software libraries, including: cclib¹² for parsing of result files, VMD¹³/Tachyon¹⁴ for 3D rendering, Matplotlib¹⁵ for drawing of graphs, Open Babel¹⁶/Pybel¹⁷ for file interconversion and PySOC¹⁸ for the calculation of spin-orbit coupling.

Electrochemistry measurements.

Cyclic Voltammetry (CV) analysis was performed on an Electrochemical Analyzer potentiostat model 620E from CH Instruments at a sweep rate of 100 mV/s. Differential pulse voltammetry (DPV) was conducted with an increment potential of 0.01 V and a pulse amplitude, width, and period of 50 mV, 0.06, and 0.5 s, respectively. All measurements were performed in degassed MeCN with 0.1 M tetra-*n*-butylammonium hexafluorophosphate ([^{*n*}Bu₄N]PF₆) as the supporting electrolyte and ferrocene/ferrocenium (Fc/Fc⁺) as the internal reference (0.38 V vs SCE).¹⁹ An Ag/Ag⁺ electrode, a glassy carbon electrode and a platinum electrode were used as the reference electrode, working electrode and counter electrode, respectively. The HOMO and LUMO energies were determined using the relation the relation HOMO/LUMO = $-(E_{\text{ox}}/E_{\text{red}} \text{ vs Fc/Fc}^+ + 4.8)$,^{20, 21} where E_{ox} and E_{red} are the oxidation and reduction peak potentials versus Fc/Fc⁺, respectively, calculated from the DPV.

Photophysical measurements:

Optically dilute solutions of concentrations on the order of 10⁻⁵ M were prepared in HPLC grade solvent for absorption and emission analysis. Absorption spectra were recorded at room temperature on a Shimadzu UV-2600 double beam spectrophotometer. Molar absorptivity determination was verified by linear regression analysis of values obtained from five independent solutions at varying concentrations around 10⁻⁵ M. For emission studies, steady-

state photoluminescence (SS PL) spectra and time-resolved PL decays in solution were recorded at 298 K using Edinburgh Instruments FS5 fluorophotometer. Degassed solutions were prepared via three freeze-pump-thaw cycles and spectra/decays were measured using a home-made Schlenk quartz cuvette. Samples were excited at 340 nm for steady-state measurements. Time-resolved PL measurements of solutions were carried out using the time-correlated single-photon counting (TCSPC) technique. The samples were excited at 375 nm with a pulsed laser diode. Photoluminescence quantum yields for solutions were determined using the optically dilute method,²² in which four sample solutions with absorbances between 0.3 to 0.09 at 350 nm were used. The Beer-Lambert law was found to remain linear at the concentrations of the solutions. For each sample, linearity between absorption and emission intensity was verified through linear regression analysis with the Pearson regression factor (R^2) for the linear fit of the data set surpassing 0.9. Individual relative quantum yield values were calculated for each solution and the values reported represent the average of these results. The quantum yield of the sample, Φ_{PL} , can be determined by the equation $\Phi_{PL} = \left(\Phi_r * \frac{A_r}{A_s} * \frac{I_s}{I_r} * \frac{n_s^2}{n_r^2} \right)$, where A stands for the absorbance at the excitation wavelength (λ_{exc} : 350 nm), I is the integrated area under the corrected emission curve and n is the refractive index of the solvent with the subscripts “s” and “r” representing sample and reference respectively.²³ Φ_r is the absolute quantum yield of the external reference quinine sulfate ($\Phi_r = 54.6\%$ in 0.5 M H_2SO_4).²⁴ The experimental uncertainty in the PL quantum yields is conservatively estimated to be 10%, though we have found that statistically we can reproduce Φ_{PL} values to 3% relative error.

Thin doped films of emitters in a host matrix were spin-coated on a quartz substrate using a spin speed of 1500 rpm for 60 s to give a thickness of ~80 nm. An integrating sphere (Edinburgh Instruments FS5, SC30 module) was employed for quantum yield measurements for thin film samples. The Φ_{PL} of the films were then measured in air and in N_2 by purging the integrating sphere with N_2 gas flow for 2 min. The photophysical properties of the film samples were measured using an Edinburgh Instruments FS5 fluorimeter. Time-resolved PL measurements of the thin films were carried out using the multi-channel scaling (MCS) and TCSPC technique.

The samples were excited at 375 nm by a pulsed laser diode for TCSPC and by a xenon flashlamp for MCS and were kept in a vacuum of $< 8 \times 10^{-4}$ mbar. The singlet-triplet splitting energy ΔE_{ST} of solutions and films were estimated from the onsets of the SS PL and phosphorescence spectra at 77 K. Samples were excited by a xenon flashlamp emitting at 340 nm (EI FS5, SC-70). Phosphorescence spectra were measured with a time-gated window of 1-10 ms.

Fitting of the time-resolved PL decays:

Time-resolved PL measurements were fitted to a sum of exponentials decay model, with chi-squared (χ^2) values between 1 and 2, using the EI FS5 software. Each component of the decay is assigned a weight, (w_i), which is the contribution of the emission from each component to the total emission.

The average lifetime was then calculated using the following:

- Two exponential decay model:

$$\tau_{AVG} = \tau_1 w_1 + \tau_2 w_2$$

with weights defined as $w_1 = \frac{A_1 \tau_1}{A_1 \tau_1 + A_2 \tau_2}$ and $w_2 = \frac{A_2 \tau_2}{A_1 \tau_1 + A_2 \tau_2}$ where A_1 and A_2 are the preexponential-factors of each component.

- Three exponential decay model:

$$\tau_{AVG} = \tau_1 w_1 + \tau_2 w_2 + \tau_3 w_3$$

with weights defined as $w_1 = \frac{A_1 \tau_1}{A_1 \tau_1 + A_2 \tau_2 + A_3 \tau_3}$, $w_2 = \frac{A_2 \tau_2}{A_1 \tau_1 + A_2 \tau_2 + A_3 \tau_3}$ and $w_3 = \frac{A_3 \tau_3}{A_1 \tau_1 + A_2 \tau_2 + A_3 \tau_3}$ where A_1 , A_2 and A_3 are the preexponential-factors of each component.

OLED Fabrication and Characterization:

The solution-processed devices with **2,7-tBuCzNB** were fabricated as follows. Patterned ITO substrates were irradiated with UV-O₃ for 30 min. PEDOT:PSS (CH 8000) mixed with ultra-pure water (1:1) was spin-coated onto the ITO substrate at 500 rpm for 1 s, 4000 rpm for 12 s, and then 500 rpm for 1 s followed by annealing at 150 °C for 10 min in air. Afterward, PVK dissolved in *o*-dichlorobenzene (10 mg/mL) was spin-coated at 2000 rpm for 30 s and baked at 120 °C for 10 min in air. Then, the emitter and DMIC-TRZ or mCP: 1,3-bis[2-(4-*tert*-butylphenyl)-1,3,4-oxadiazole-5-yl]benzene (OXD-7), dissolved in chlorobenzene (10 mg/mL), were spin-coated and annealed in a vacuum oven under the condition shown in Table S1. Then, the ITO substrate with these layers was transferred to the vacuum deposition chamber (C-E2L1G1, Choshu Industry Co., Ltd., Japan) to vacuum deposit PO-T2T (20 nm), B4PyMPM (35 nm), and LiF (1 nm) in an organic chamber under 10⁻⁵ Pa, and finally Al (100 nm) in an inorganic chamber under 10⁻⁴ Pa. The performance of OLEDs was characterized employing an integrating sphere integrated with an absolute EQE measurement system (C9920-12, Hamamatsu Photonics, Japan) equipped with a source meter (2400, Keithley, Japan). These measurements were conducted in the forward direction in 200 mV steps.

Table S1. The conditions of spin-coating and annealing for the emission layers.

Host material	Doped concentration	Spin-coating	Annealing
DMIC-TRZ	5 wt%	1500 rpm, 30 s	100 °C, 10 min
	10 wt%	1500 rpm, 30 s	100 °C, 10 min
mCP:OXD-7	5 wt%	2200 rpm, 30 s	50 °C, 10 min
	10 wt%	3000 rpm, 30 s	50 °C, 10 min

Synthesis:

2,7-dibromo-9-(*tert*-butyldimethylsilyl)-9*H*-carbazole (1)

NaH (60% dispersion in mineral oil, 0.74 g, 18.5 mmol, 1.2 equiv.) was slowly added to a

solution of 2,7-dibromo-9H-carbazole (5.00 g, 15.4 mmol, 1 equiv.) in THF (50 mL) at 0 °C. After stirring for 30 min, *tert*-butyldimethylsilyl chloride (2.78 g, 18.5 mmol, 1.2 equiv.) was added and the mixture was stirred at room temperature under nitrogen for 3 h. The reaction was quenched by adding water and extracted with 3× 50 mL dichloromethane. The combined organic phase was then concentrated under reduced pressure. The crude material was recrystallized from methanol to afford **1** as a white amorphous solid. **Yield** 93%, 6.30 g. **Mp**: 160-161 °C. **R_f**: 0.6 (ethyl acetate: hexane = 1: 5). **¹H NMR (400 MHz, CDCl₃)** δ 7.86 (d, J = 8.3 Hz, 2H), 7.72 (d, J = 1.3 Hz, 2H), 7.35 (dd, J = 8.3, 1.6 Hz, 2H), 1.04 (s, 9H), 0.76 (s, 6H). **¹³C NMR (101 MHz, CDCl₃)** δ 146.13, 124.74, 123.38, 120.97, 119.34, 117.29, 26.64, 20.61, -1.13. **HRMS (MALDI-MS):** [C₁₈H₂₁Br₂NSi]⁺ **Calculated:** 436.9805; **Found:** 436.9792.

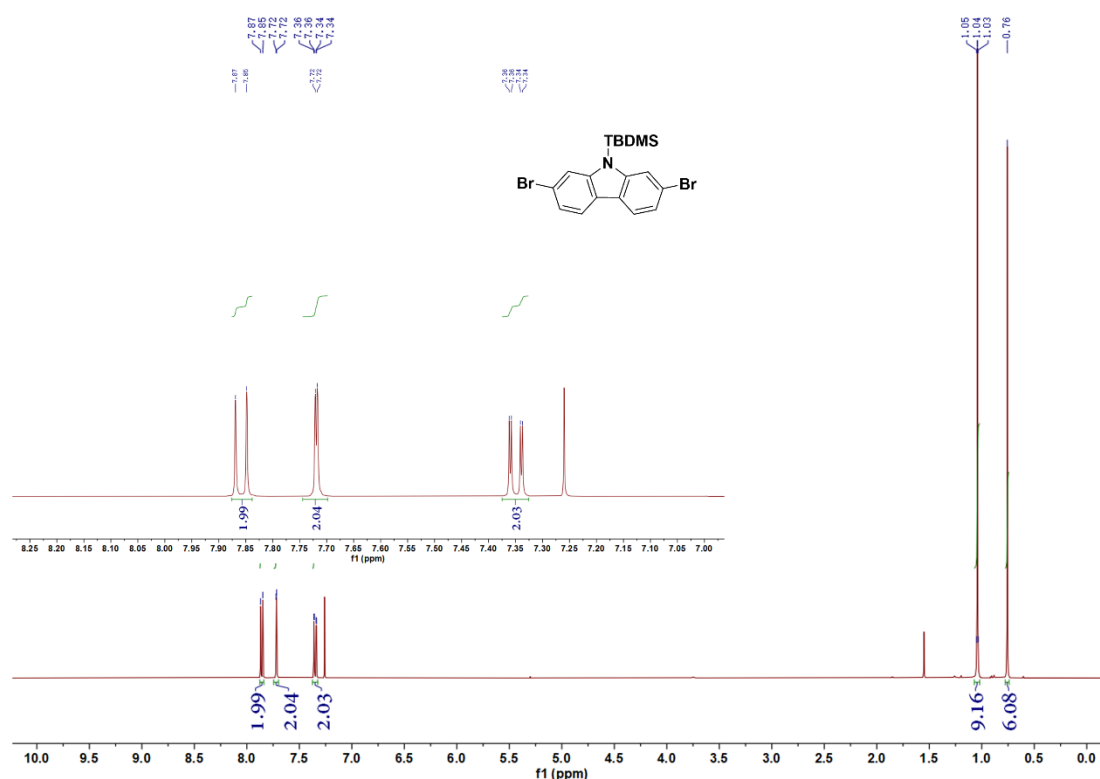


Figure S1. ¹H NMR spectrum of **1** in CDCl₃.

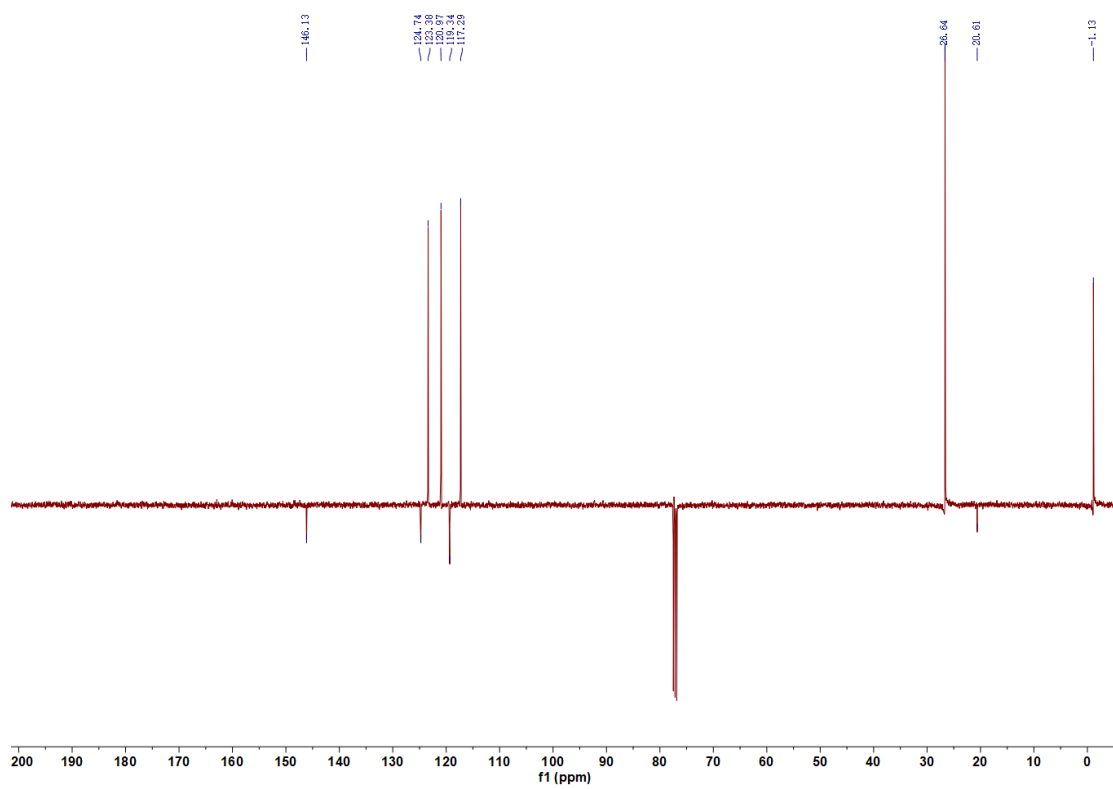


Figure S2. DEPTQ ^{13}C NMR spectrum of **1** in CDCl_3 .

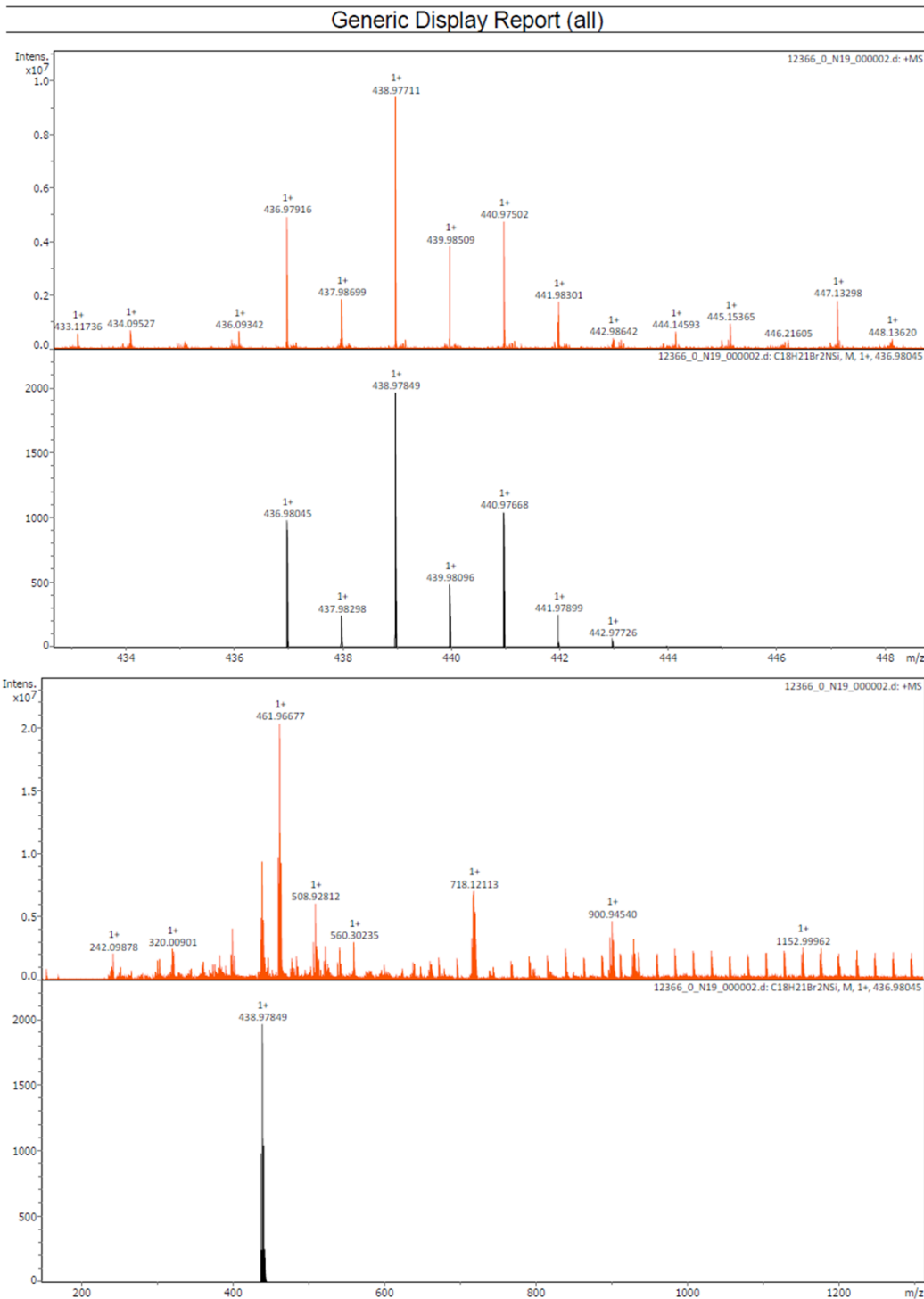


Figure S3. MALDI-HRMS spectrum of 1.

3,3'',6,6''-tetra-*tert*-butyl-9'-(*tert*-butyldimethylsilyl)-9'*H*-9,2':7',9''-tercarbazole (2)

3,6-di-*tert*-butyl-9*H*-carbazole (4.20 g, 15.0 mmol, 2.2 equiv.), Compound 1 (3.00 g, 6.83 mmol, 1.0 equiv.), Pd₂(dba)₃ (188 mg, 0.205 mmol, 0.03 equiv.), tri-*tert*-butylphosphonium

tetrafluoroborate (159 mg, 0.546 mmol, 0.08 equiv.), NaO^tBu (1.97 g, 20.5 mmol, 3 equiv.) were added into toluene (35 mL). The mixture was stirred at 115°C for 72 h under a nitrogen atmosphere. After cooling to room temperature, the reaction was quenched with 50 mL water and extracted with 3× 50 mL dichloromethane. The combined organic phase was then concentrated under reduced pressure. The product was purified by column chromatography on silica gel (dichloromethane: hexane = 1: 15) to give **2** as a white amorphous powder. **Yield** 81%, 4.65 g. **Mp**: 253-254 °C. **R_f**: 0.3 (dichloromethane: hexane = 1: 5). **¹H NMR (400 MHz, CDCl₃)** δ 8.27 (d, J = 8.2 Hz, 2H), 8.19 (d, J = 1.5 Hz, 4H), 7.81 (d, J = 1.4 Hz, 2H), 7.49 (dd, J = 8.7, 1.9 Hz, 4H), 7.46 (dd, J = 8.2, 1.6 Hz, 2H), 7.42 (d, J = 8.6 Hz, 4H), 1.50 (s, 36H), 1.05 (s, 9H), 0.74 (s, 6H). **¹³C NMR (101 MHz, CDCl₃)** δ 146.48, 142.87, 139.74, 135.60, 125.01, 123.76, 123.43, 120.77, 119.24, 116.43, 112.81, 109.37, 34.92, 32.21, 26.63, 20.61, -0.87. **HRMS (ESI-MS): [C₅₈H₆₉N₃Si + H]⁺ Calculated: 836.5334; Found: 836.5293.**

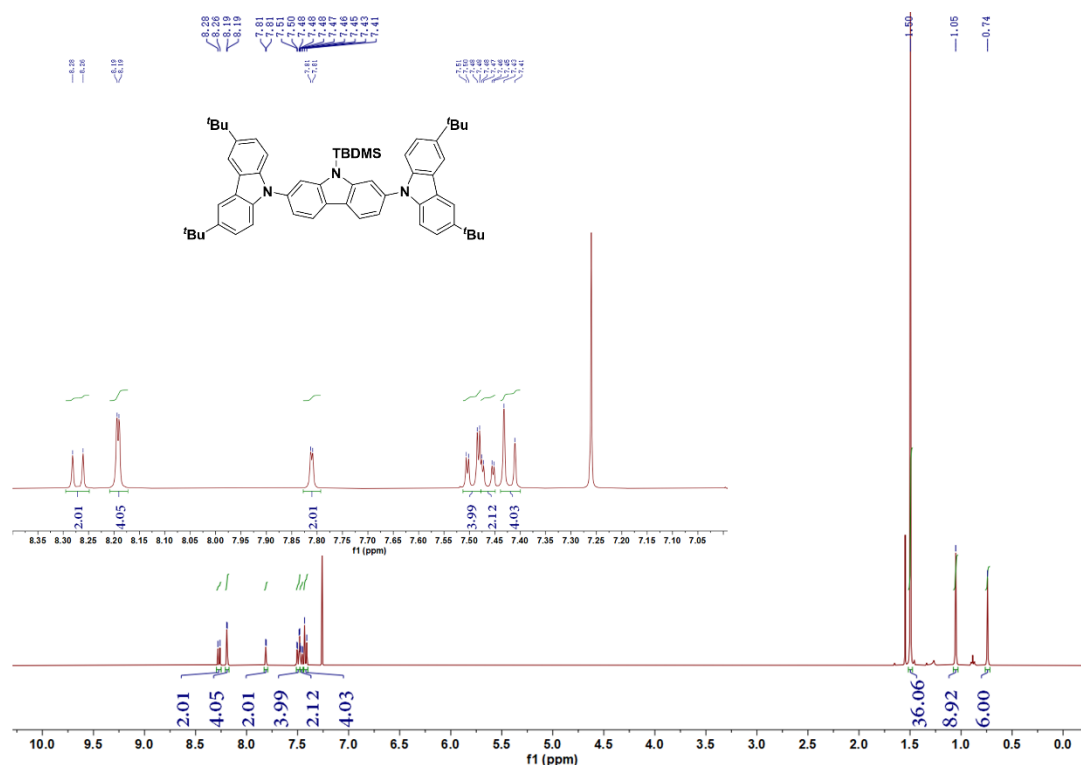


Figure S4. ¹H NMR spectrum of **2** in CDCl₃.

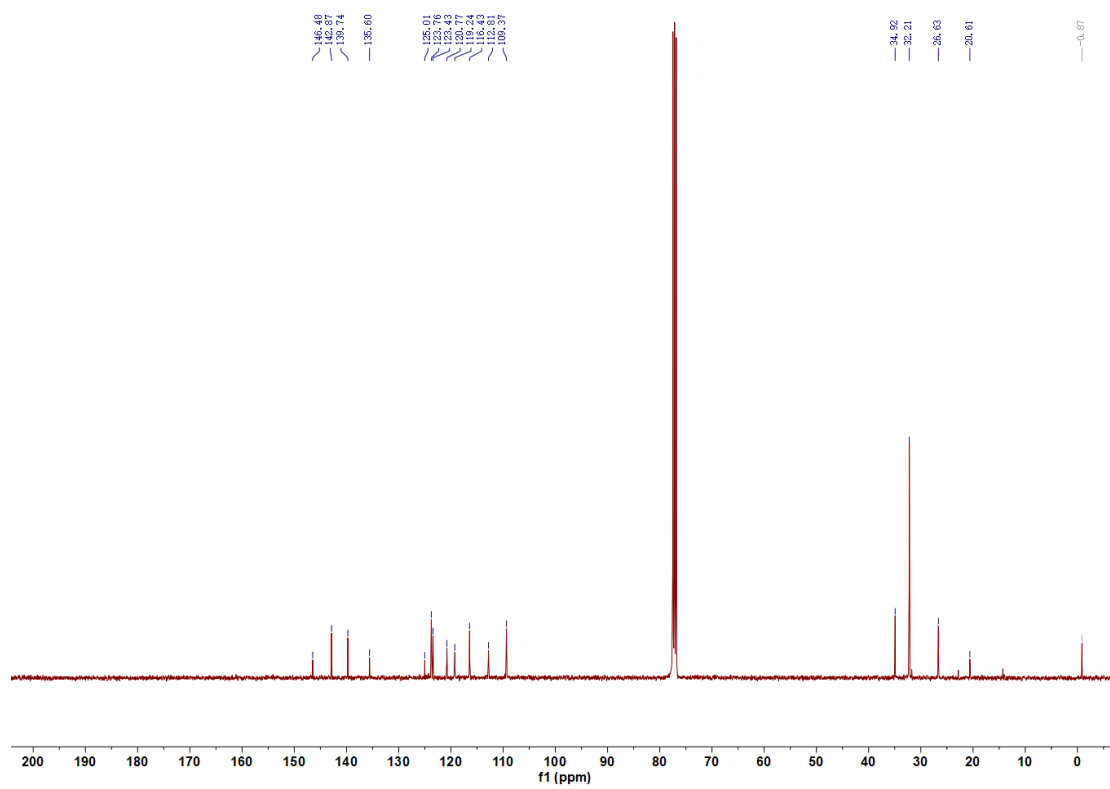


Figure S5. ^{13}C NMR spectrum of **2** in CDCl_3 .

Display Report

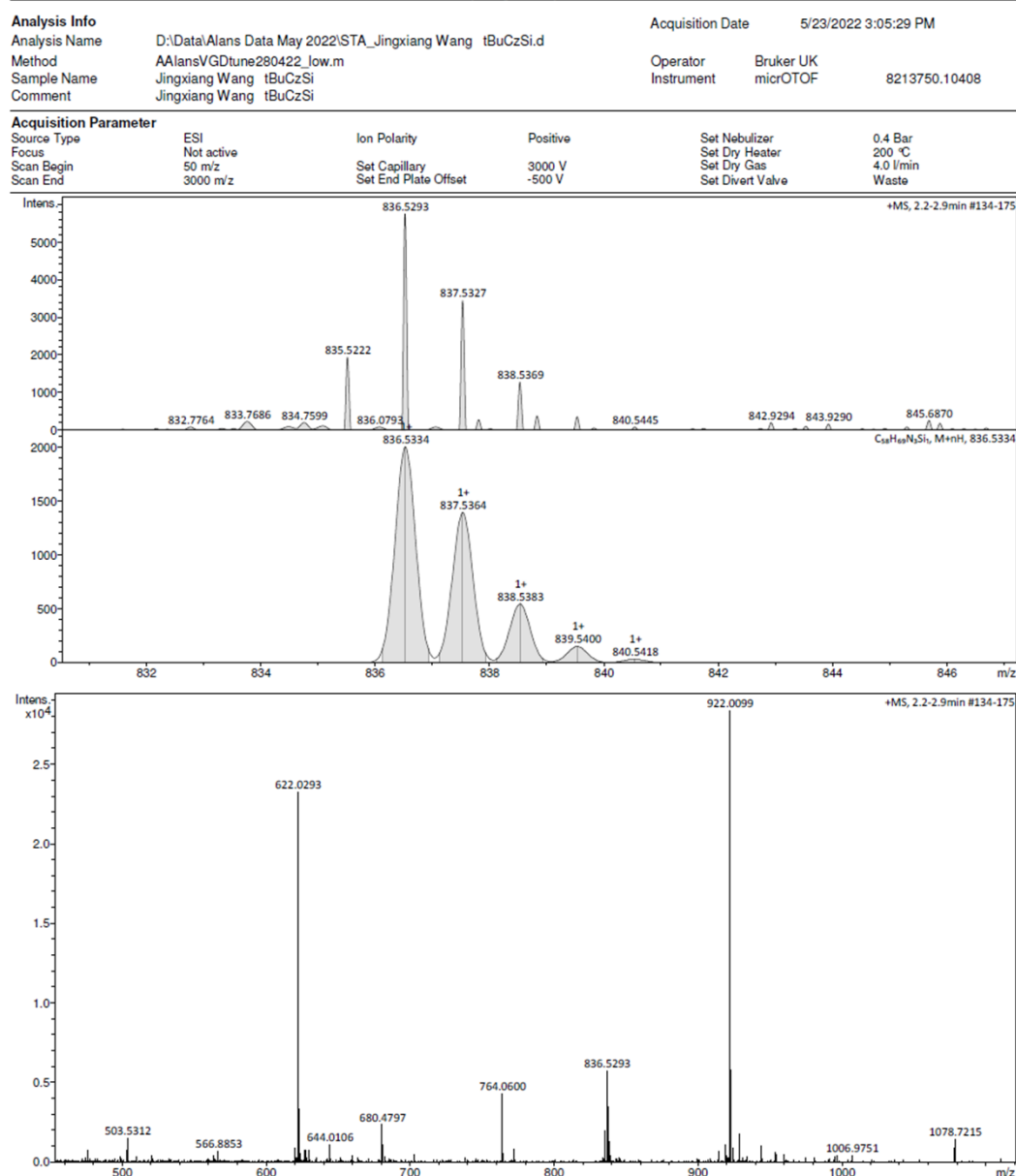


Figure S6. ESI-HRMS spectrum of **2**.

3,3'',6,6''-tetra-*tert*-butyl-9'*H*-9,2':7',9''-tercarbazole (**3**)

Compound **2** (1.70 g, 2.03 mmol, 1.0 equiv.) was dissolved in toluene (15 mL), then TBAF (1.0 M THF solution, 3.05 mL, 1.5 equiv.) was added dropwise. The solution was stirred under a nitrogen atmosphere for 2.5 h. After adding NH₄Cl (5.0 M aqueous solution, 8.2 mL) to the reaction mixture, the mixture was extracted with 3 × 50 mL dichloromethane. The combined organic phase was concentrated under reduced pressure. The crude material was washed with

hexane and methanol to afford **3** as a white amorphous solid. **Yield** 91%, 1.33 g. **Mp**: >395 °C. **R_f**: 0.5 (ethyl acetate: hexane = 1: 5). **¹H NMR (400 MHz, THF-*d*⁸)** δ 10.86 (s, 1H), 8.37 (d, J = 8.2 Hz, 2H), 8.23 (d, J = 1.6 Hz, 4H), 7.69 (d, J = 1.6 Hz, 2H), 7.47 (dd, J = 8.7, 1.9 Hz, 4H), 7.42 (dd, J = 8.2, 1.8 Hz, 2H), 7.39 (d, J = 8.6 Hz, 4H), 1.47 (s, 36H). **¹³C NMR (101 MHz, THF-*d*⁸)** δ 143.39, 142.84, 141.01, 137.10, 124.55, 124.41, 123.22, 122.24, 119.33, 117.16, 110.32, 110.22, 35.52, 32.57. **HRMS (ESI-MS): [C₅₂H₅₅N₃ +H]⁺ Calculated: 722.4469; Found: 722.4472.**

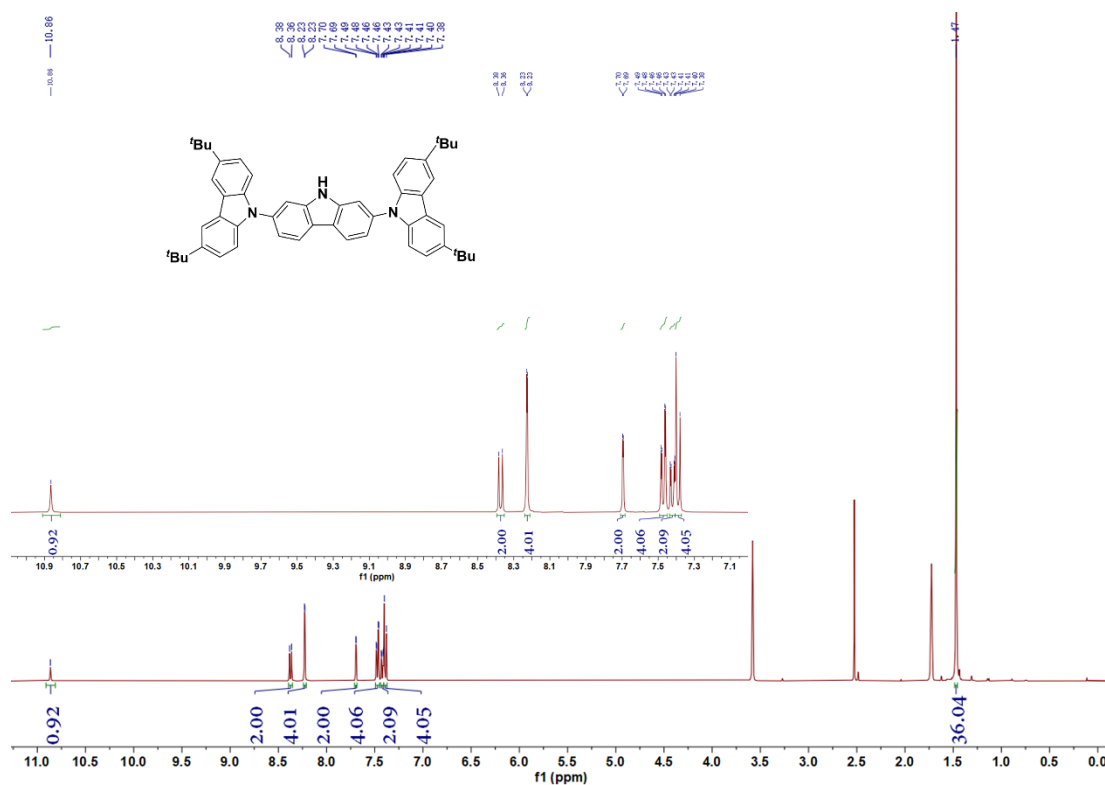


Figure S7. ¹H NMR spectrum of **3** in THF-*d*⁸.

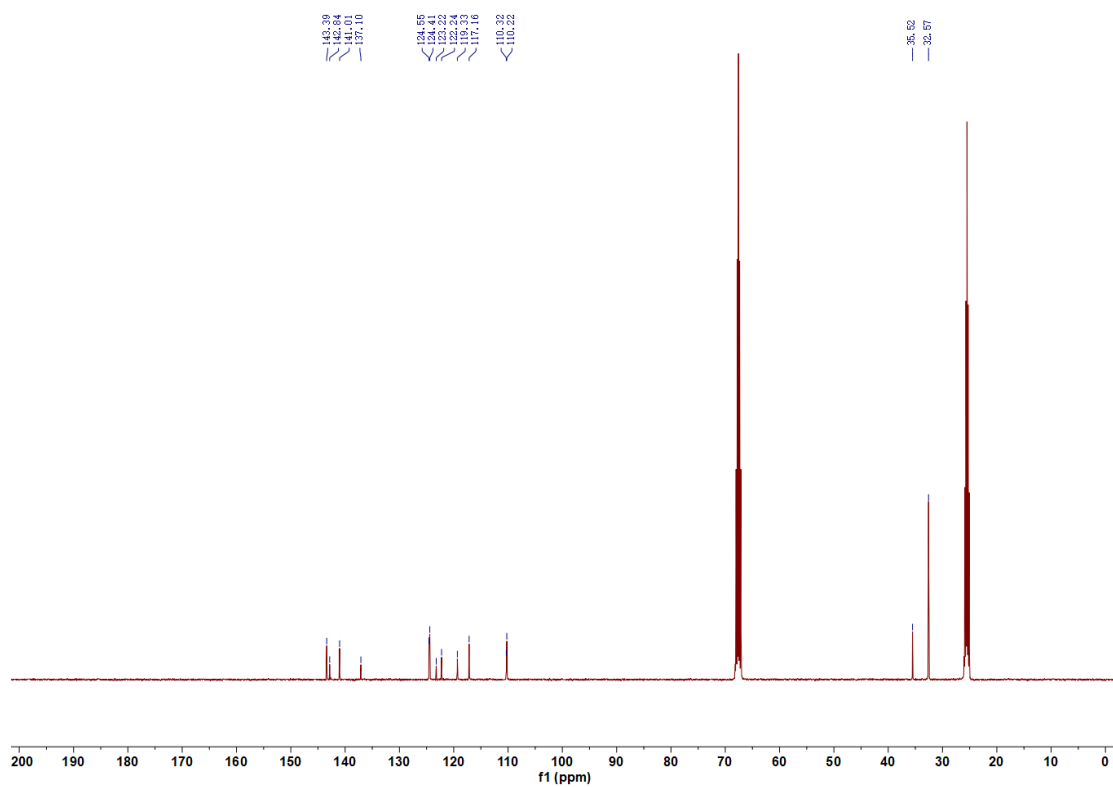


Figure S8. ^{13}C NMR spectrum of **3** in $\text{THF-}d^8$.

Display Report

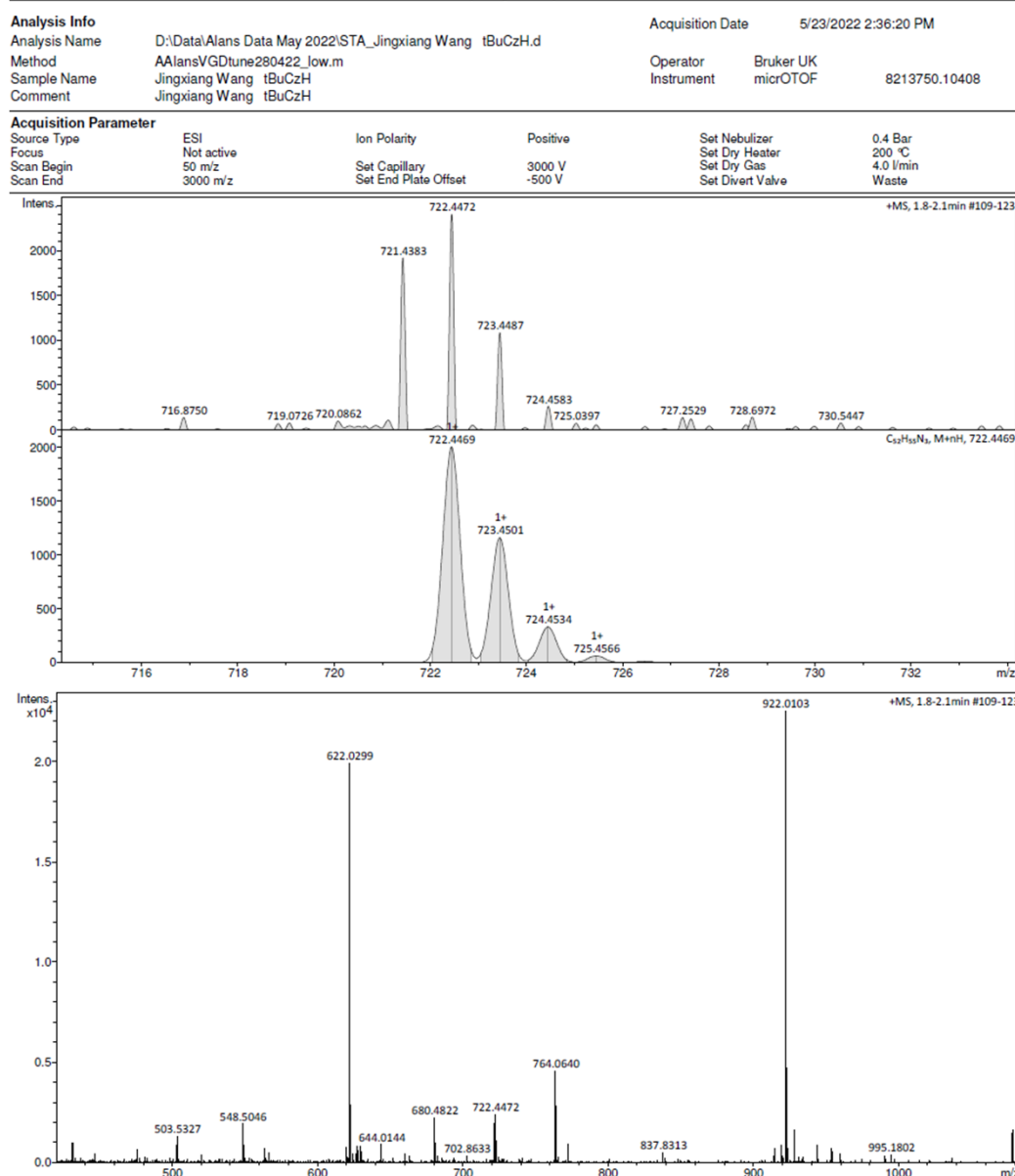


Figure S9. ESI-HRMS spectrum of **3**.

9',9''''-(2-bromo-1,3-phenylene)bis(3,3'',6,6''-tetra-*tert*-butyl-9'*H*-9,2':7',9''-tercarbazole) (4)

3 (1.26 g, 1.74 mmol, 2.1 equiv.), 2-bromo-1,3-difluorobenzene (93.0 μ L, 0.829 mmol, 1 equiv.), caesium carbonate (1.35 g, 4.15 mmol, 5 equiv.) and DMF (25 mL) were added to a 2-neck Schlenk tube. The mixture was stirred at 155 °C under nitrogen for 72 h. After cooling to room temperature, the reaction mixture was poured into water and extracted with 3 \times 50 mL

dichloromethane. The combined organic phase was then concentrated under reduced pressure and the crude product was purified by column chromatography on silica gel (dichloromethane: hexane = 1: 5) and washed with MeOH to give **4** as a white amorphous powder. **Yield** 35%, 467 mg. **Mp**: 336-338 °C. **R_f**: 0.25 (dichloromethane: hexane = 1: 4.5). **¹H NMR (500 MHz, THF-*d*⁸)** δ 8.52 (d, J = 8.2 Hz, 4H), 8.10 (s, 8H), 7.89 (d, J = 8.0 Hz, 2H), 7.74 – 7.70 (m, 1H), 7.57 (dd, J = 8.2, 1.6 Hz, 4H), 7.48 (d, J = 1.3 Hz, 4H), 7.29 (d, J = 6.5 Hz, 8H), 7.11 (s, 8H), 1.31 (s, 72H). **¹³C NMR (126 MHz, THF-*d*⁸)** δ 143.45, 143.30, 140.45, 139.47, 137.75, 132.84, 131.63, 125.59, 124.55, 124.51, 123.04, 122.45, 120.48, 117.14, 110.17, 109.55, 35.41, 32.49. **HRMS (ESI-MS):** [C₁₁₀H₁₁₁BrN₆ + H]⁺ **Calculated:** 1595.8126; **Found:** 1595.8114.

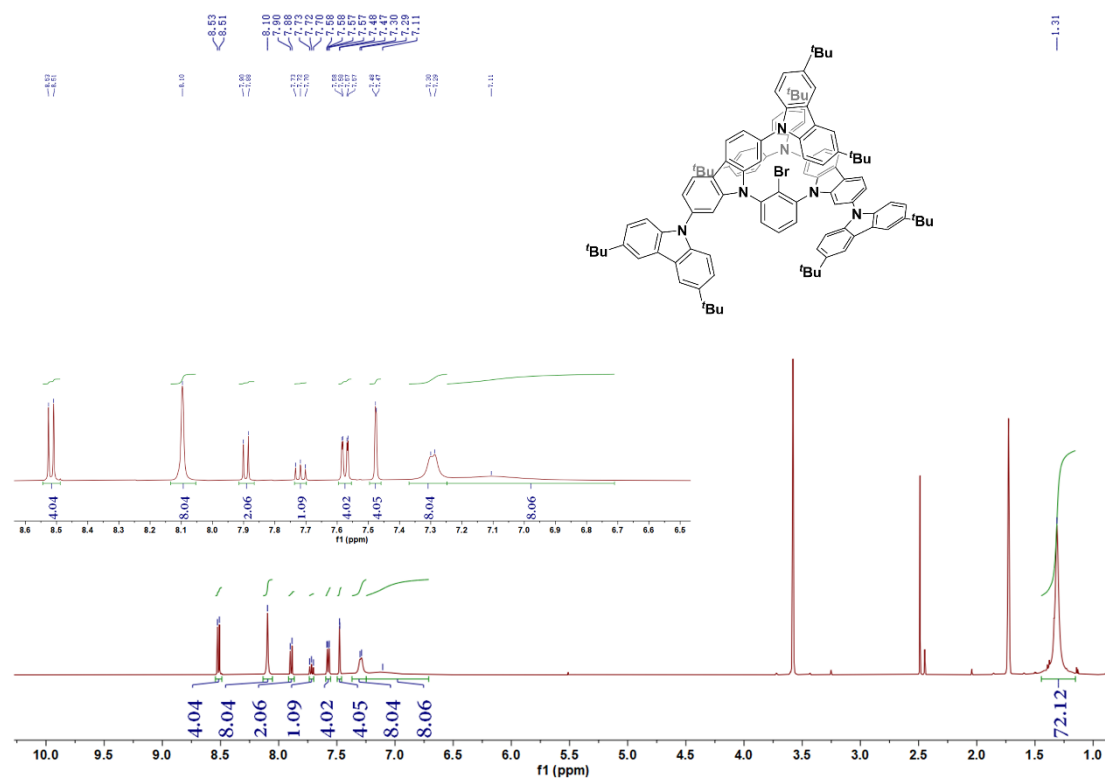


Figure S10. ¹H NMR spectrum of **4** in THF-*d*⁸.

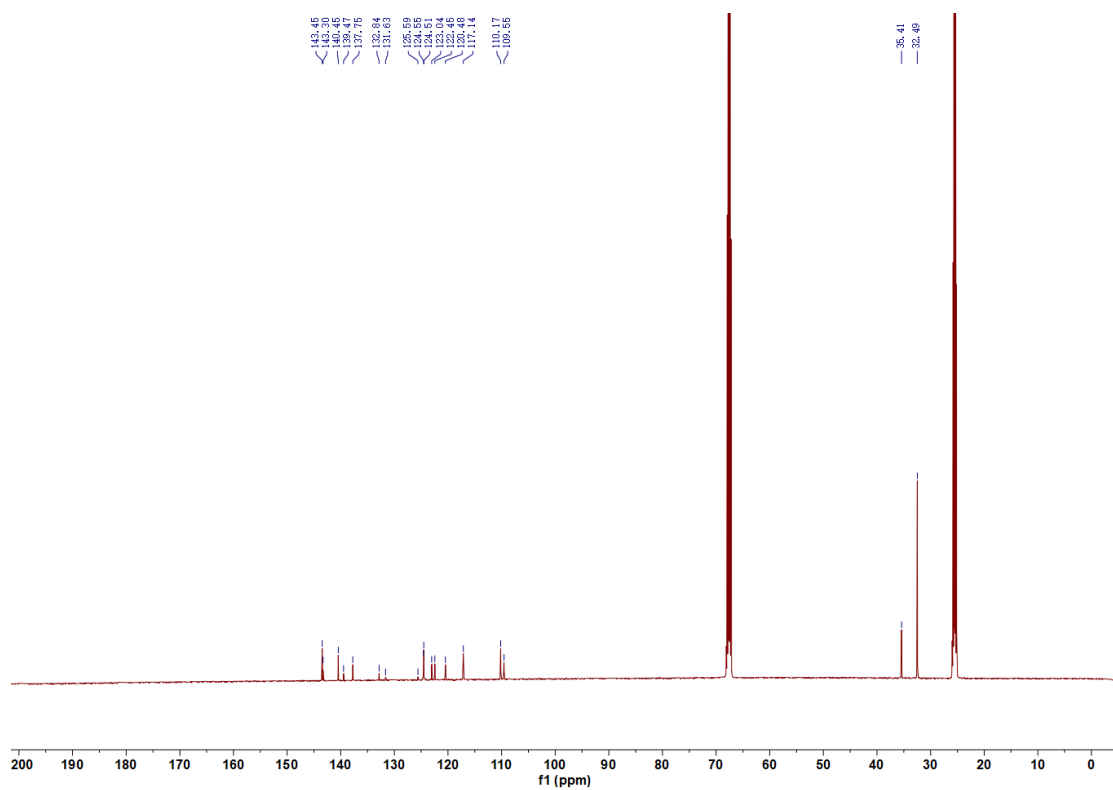


Figure S11. ^{13}C NMR spectrum of 4 in $\text{THF-}d^8$.

Display Report

Analysis Info		Acquisition Date		4/14/2022 2:32:08 PM	
Analysis Name	D:\Data\Alans Data April 2022\STA_Jingxiang Wang tBuCzCzPhBr.d	Operator	Bruker UK		
Method	020216alanstune_MED.m	Instrument	micrOTOF	8213750.10408	
Sample Name	Jingxiang Wang tBuCzCzPhBr				
Comment	Jingxiang Wang tBuCzCzPhBr				
Acquisition Parameter					
Source Type	ESI	Ion Polarity	Positive	Set Nebulizer	0.4 Bar
Focus	Not active	Set Capillary	3500 V	Set Dry Heater	230 °C
Scan Begin	30 m/z	Set End Plate Offset	-500 V	Set Dry Gas	6.0 l/min
Scan End	3000 m/z			Set Divert Valve	Waste

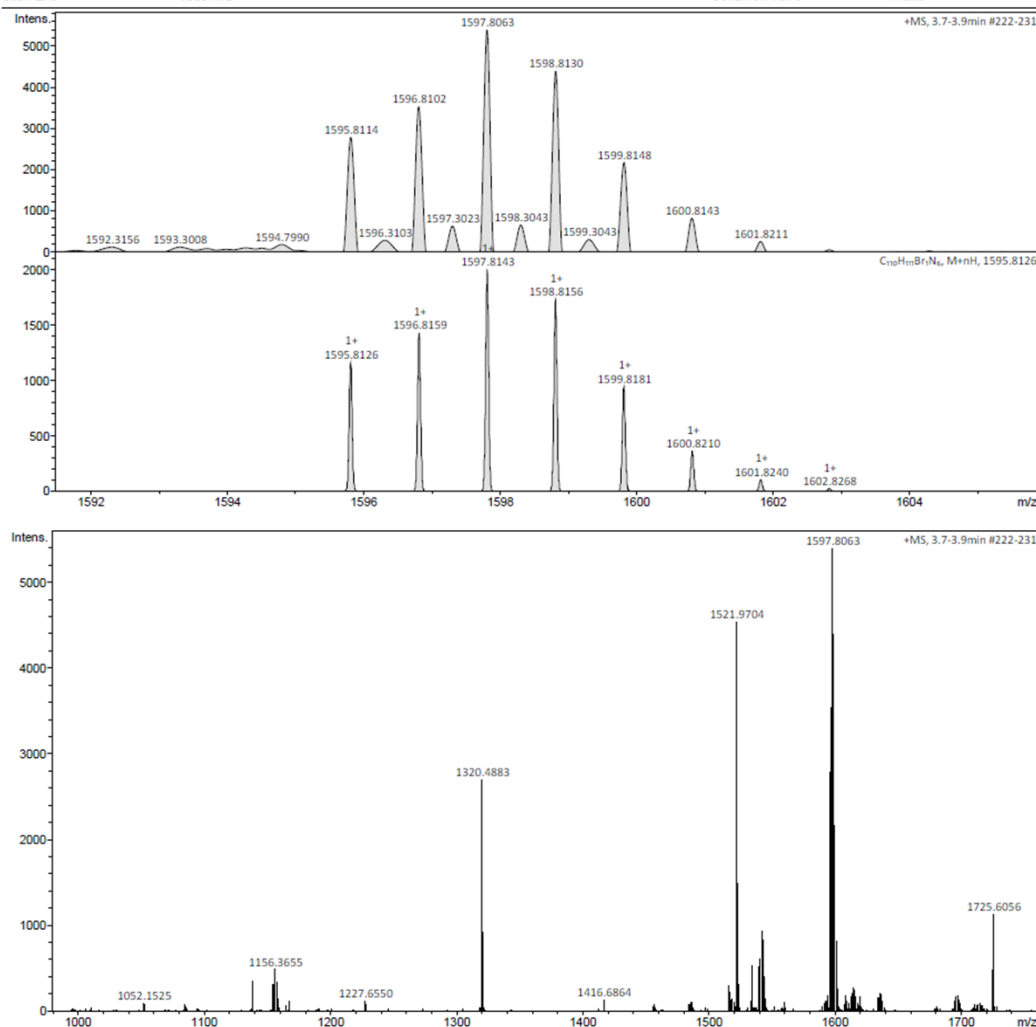


Figure S12. ESI-HRMS spectrum of **4**.

2,7-tBuCzNB

To a solution of **4** (200 mg, 0.125 mmol, 1.0 equiv.) in *tert*-butylbenzene (10 mL) at $-78\text{ }^{\circ}\text{C}$ under a nitrogen atmosphere was added slowly a solution of *tert*-butyllithium in pentane (294.7 μL , 1.7 M, 4.43 mmol, 4 equiv.). The reaction mixture was then allowed to warm to room temperature. After heating and stirring at $65\text{ }^{\circ}\text{C}$ for 4 h, the reaction was then cooled to $-78\text{ }^{\circ}\text{C}$ and borontribromide (47.4 μL , 0.501 mmol, 4 equiv.) was added slowly. The reaction mixture

was allowed to warm to room temperature for 24 h and then *N,N*-diisopropylethylamine (131 μL , 0.751 mmol, 6 equiv.) was added at 0 $^{\circ}\text{C}$. After heating and stirring at 180 $^{\circ}\text{C}$ for 2 days, the reaction was quenched by water and extracted with 3 \times 50 mL dichloromethane. The combined organic phase was then concentrated under reduced pressure. The crude product was purified by column chromatography on silica gel (dichloromethane: hexane = 1: 7) to afford **2,7-tBuCzNB** as a yellow amorphous powder. **Yield** 12%, 23 mg. **Mp**: decomposed at around 340 $^{\circ}\text{C}$. **R_f**: 0.3 (dichloromethane: hexane = 1: 4). **¹H NMR (500 MHz, THF-*d*⁸)** δ 8.96 – 8.86 (m, 4H), 8.83 (d, *J* = 8.8 Hz, 1H), 8.60 (d, *J* = 8.2 Hz, 1H), 8.46 (d, *J* = 1.8 Hz, 1H), 8.38 (d, *J* = 8.1 Hz, 3H), 8.23 (d, *J* = 1.6 Hz, 2H), 8.04 (d, *J* = 1.6 Hz, 4H), 7.97 – 7.90 (m, 2H), 7.85 (dd, *J* = 8.7, 2.0 Hz, 1H), 7.74 – 7.68 (m, 2H), 7.66 (s, 2H), 7.45 – 7.36 (m, 6H), 7.20 (s, 4H), 7.02 (s, 4H), 1.52 (s, 9H), 1.44 (s, 18H), 1.39 (s, 36H), 1.06 (s, 9H). **¹³C NMR (126 MHz, THF-*d*⁸)** δ 147.01, 146.00, 145.86, 145.32, 144.76, 143.52, 143.27, 142.42, 142.36, 142.24, 141.11, 140.63, 140.37, 139.05, 137.55, 136.58, 134.72, 129.26, 128.77, 127.09, 126.81, 125.66, 125.52, 124.55, 124.52, 124.41, 124.36, 124.31, 123.83, 123.38, 122.93, 122.58, 122.28, 120.61, 118.80, 118.25, 117.84, 117.14, 116.80, 115.82, 115.77, 115.12, 110.55, 110.07, 109.97, 108.85, 35.67, 35.48, 35.43, 32.51, 32.20, 31.91. **HRMS (MALDI-MS):** $[\text{C}_{110}\text{H}_{109}\text{BN}_6]^+$ **Calculated:** 1524.8801; **Found:** 1524.8826. **Anal. Calcd. For C₁₁₀H₁₀₉BN₆:** C 86.58%, H 7.20 %, N 5.51%. **Found:** C 86.65%, H 7.51%, N 5.11%. **HPLC** (82% Tetrahydrofuran and 18% Water): 98.25% pure, retention time 8.538 min.

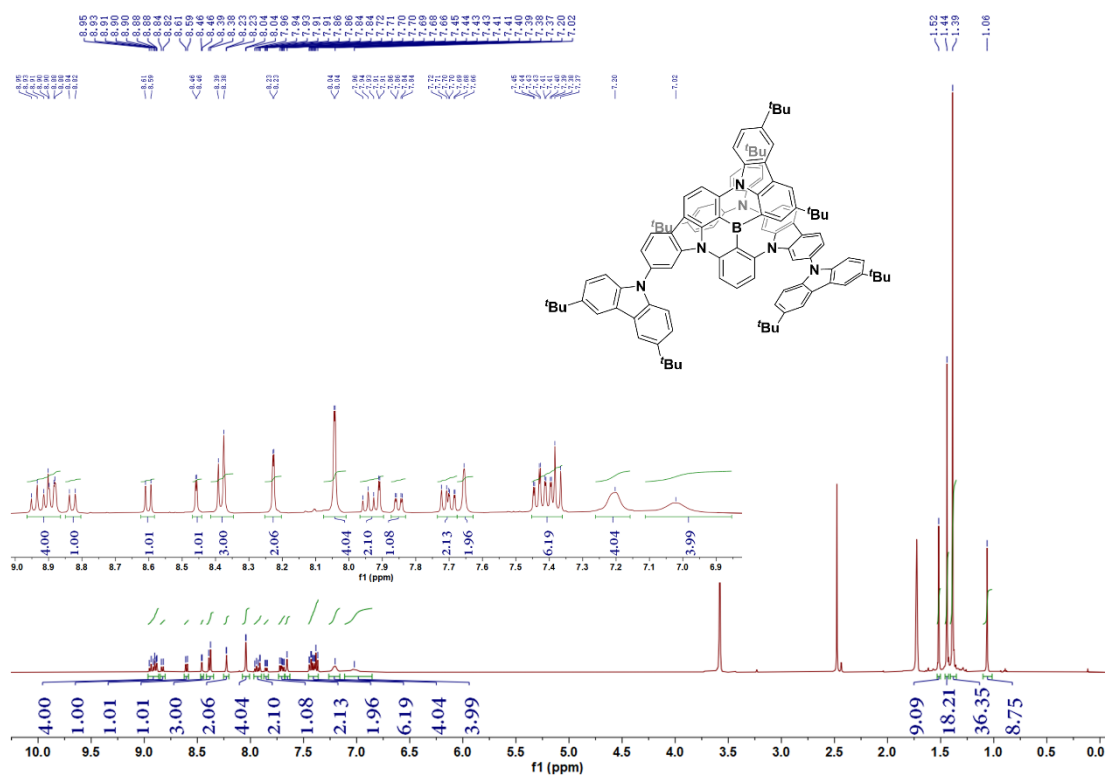


Figure S13. ^1H NMR spectrum of 2,7-tBuCzNB in THF- d^8 .

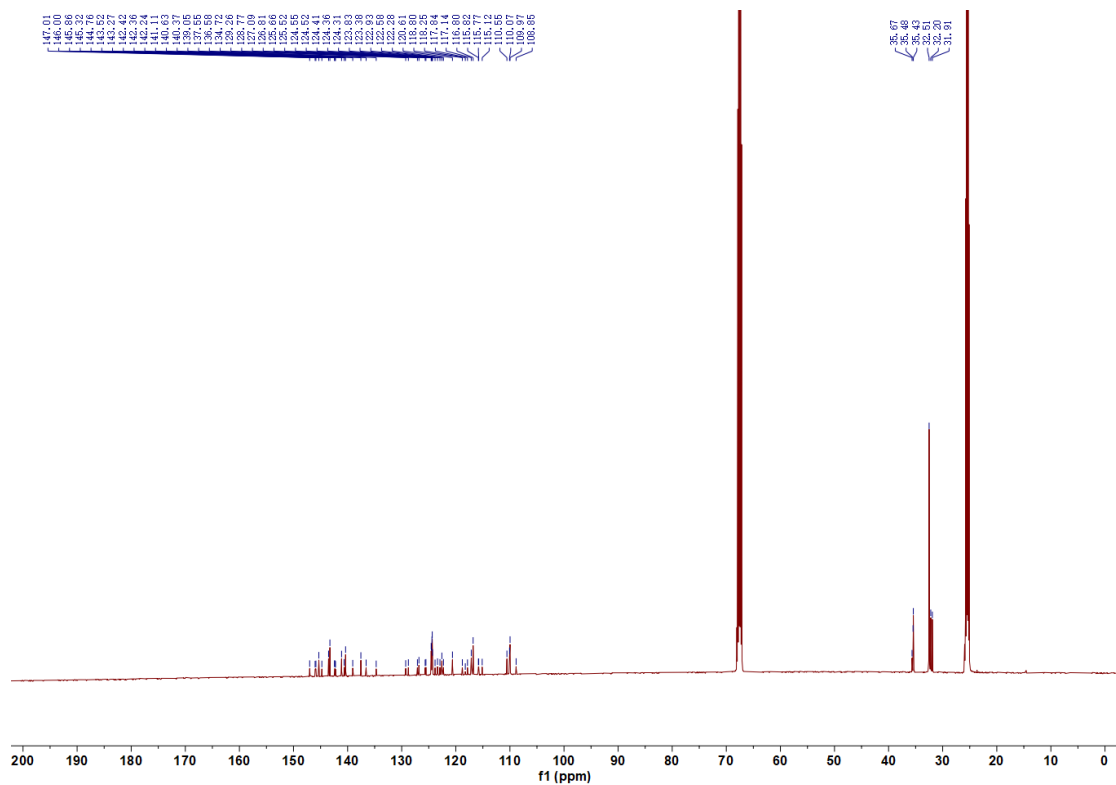


Figure S14. ^{13}C NMR spectrum of 2,7-tBuCzNB in THF- d^8 .

Window Display Report

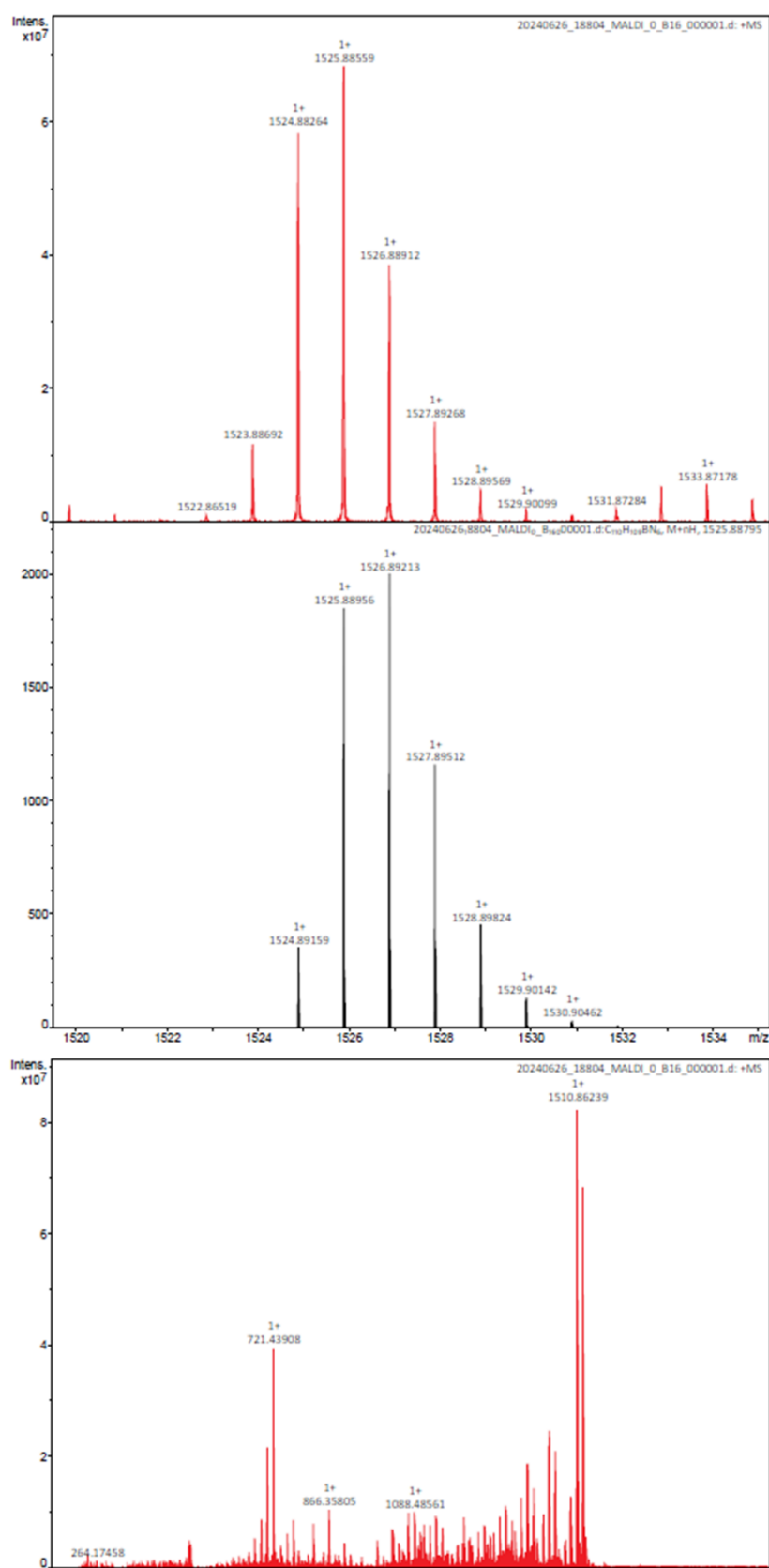


Figure S15. MALDI-TOF mass spectrum of 2,7-tBuCzNB.

Elemental Analysis Service Request Form

Researcher name Jingxiang Wang

Researcher email jw357@st-andrews.ac.uk

NOTE: Please submit ca. 10 mg of sample

Sample reference number	tBuCzBN
Name of Compound	
Molecular formula	C ₁₁ H ₁₀ BN ₆
Stability	Stable in air and in most solvents
Hazards	
Other Remarks	

Analysis type:

Single Duplicate Triplicate

Analysis Result:

Element	Expected %	Found (1)	Found (2)	Found (3)
Nitrogen	5.51	5.11	5.11	
Carbon	86.58	87.15	86.14	
Hydrogen	7.2	7.53	7.48	

Authorising Signature:

Date completed	09.05.23
Signature	J. P. C.
comments	

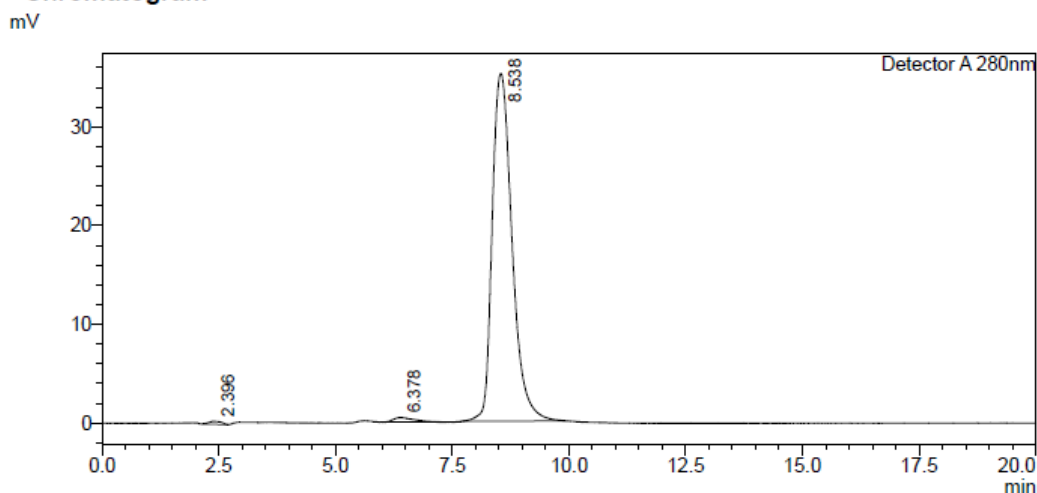
Figure S16. Elemental analysis data of 2,7-tBuCzNB.

HPLC Trace Report28Jul2023

<Sample Information>

Sample Name : tbuczbnthf4
Sample ID :
Method Filename : 82% THF 18% water 0.6 mlmin 20 mins.lcm
Batch Filename : shut down.lcb
Vial # : 2-4
Injection Volume : 2 uL
Date Acquired : 14/07/2023 19:03:52
Date Processed : 14/07/2023 19:23:54
Sample Type : Unknown
Acquired by : System Administrator
Processed by : System Administrator

<Chromatogram>



<Peak Table>

Peak#	Ret. Time	Area	Height	Area%	Area/Height	Width at 5% Height
1	2.396	5598	289	0.527	19.341	0.461
2	6.378	13046	442	1.228	29.536	0.910
3	8.538	1043601	35217	98.245	29.633	1.001
Total		1062244	35948	100.000		

Figure S17. HPLC spectrum of **2,7-tBuCzNB**.

X-ray Crystallography

A selection of crystals of **2,7-tBuCzNB** were coated in Fomblin oil, mounted on MiTeGen polyimide loops and frozen in liquid nitrogen. The mounted crystals were stored in a MiTeGen Unipuck and transported to Diamond Light Source in a cryocooled dry-shipper. Data were collected remotely²⁵ at beam line I19²⁶ of Diamond Light Source using synchrotron radiation ($\lambda = 0.6889 \text{ \AA}$) with a Si 111 double crystal monochromator, and a Dectris Pilatus 2M pixel-array photon-counting detector. Data processing used the Apex3²⁷ interface, with data reduction and scaling using SAINT²⁸ and application of a multi-scan absorption correction using

TWINABS²⁹. The structure was solved by dual-space methods (SHELXD³⁰) and refined by full-matrix least-squares against F^2 (SHELXL-2019/3³¹). Non-hydrogen atoms were refined anisotropically, and hydrogen atoms were refined using a riding model. Crystals were affected by non-merohedral twinning, showing a twin law of [1.00029 -0.05645 -0.03835 -0.00145 -1.00023 0.00186 0.01716 -0.00402 -1.00005] and a refined twin fraction of 0.4317(11). The structure showed high proportions of void space (4420 Å³) and the SQUEEZE³² routine implemented in PLATON³³ was used to remove the contribution to the diffraction pattern of the unordered electron density in the void spaces. The structure contained four independent molecules of **2,7-tBuCzNB**, all of which showed rotational disorder in at least one peripheral *tert*-butyl, and in the case of one molecule, disorder in the orientation of two di-*tert*-butylcarbazoyl groups. In all cases these were modelled using two positions and refined with geometric and thermal restraints. In most cases both components of disorder were modelled with anisotropic thermal parameters, but in cases with only a small proportion in the minor component, isotropic thermal parameters were used. All calculations except SQUEEZE were performed using the Olex2³⁴ interface. Selected crystallographic data are presented in Table S2. CCDC 2411737 contains the supplementary crystallographic data for this paper. These data can be obtained free of charge from The Cambridge Crystallographic Data Centre via www.ccdc.cam.ac.uk/structures.

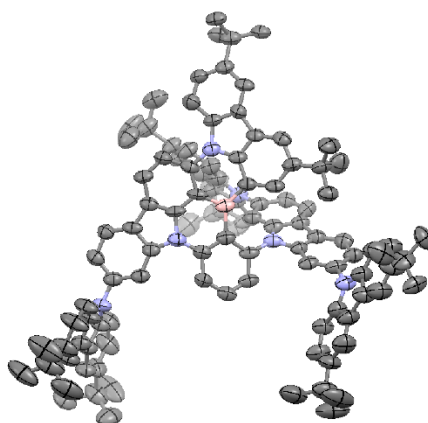


Figure S18. Thermal ellipsoid plot of the structure of one independent molecule of **2,7-tBuCzNB**. Ellipsoids are displayed at the 50% probability level, solvent molecules, minor components of disorder and hydrogen atoms are omitted for clarity.

Table S2. Selected crystallographic data.

	2,7-tBuCzNB
formula	C ₁₁₀ H ₁₀₉ BN ₆
fw	1525.84
crystal description	Yellow needle
crystal size [mm ³]	0.095×0.020×0.015
temperature [K]	100
space group	<i>P</i> $\bar{1}$
<i>a</i> [Å]	21.788(4)
<i>b</i> [Å]	26.037(5)
<i>c</i> [Å]	36.228(7)
α [°]	83.835(4)
β [°]	87.668(4)
γ [°]	87.908(3)
vol [Å ³]	20406(7)
<i>Z</i>	8
ρ (calc) [g/cm ³]	0.993
μ [mm ⁻¹]	0.054
F(000)	6528
reflections collected	268361
independent reflections (<i>R</i> _{int})	43510 (0.1458)
data/restraints/parameters	43196/1777/4572
GoF on <i>F</i> ²	1.011
<i>R</i> ₁ [<i>I</i> > 2 σ (<i>I</i>)]	0.0921
<i>wR</i> ₂ (all data)	0.2849
largest diff. peak/hole [e/Å ³]	0.342, -0.296

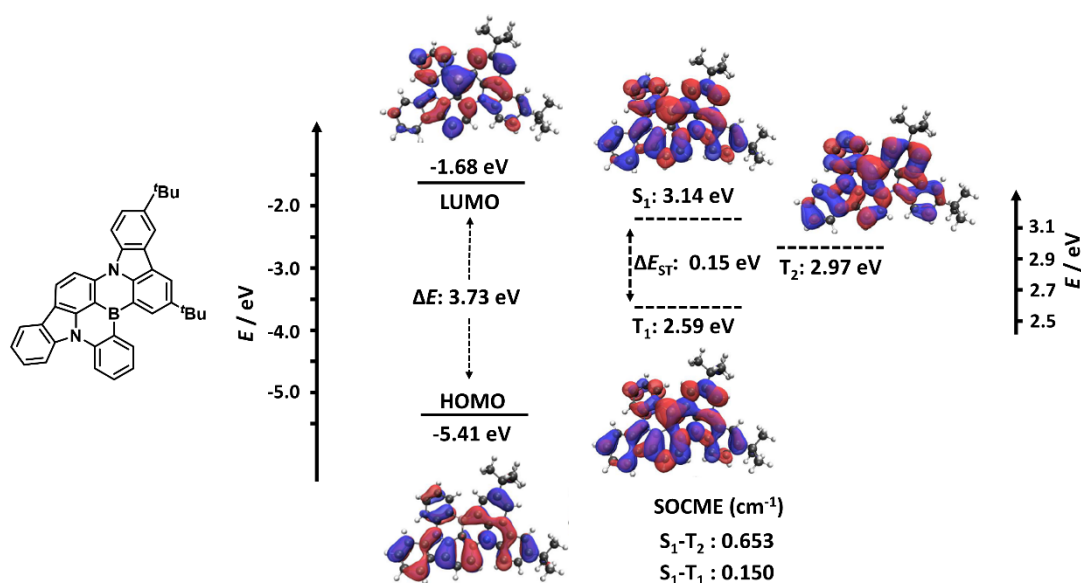


Figure S19. Calculated HOMO and LUMO energy levels and natural transition orbitals (NTOs) based on the optimized ground-state geometry and SOCME values based on the optimized T_1 geometry for Cz-SCz in the gas phase at the PBE0/6-31G(d,p) level.

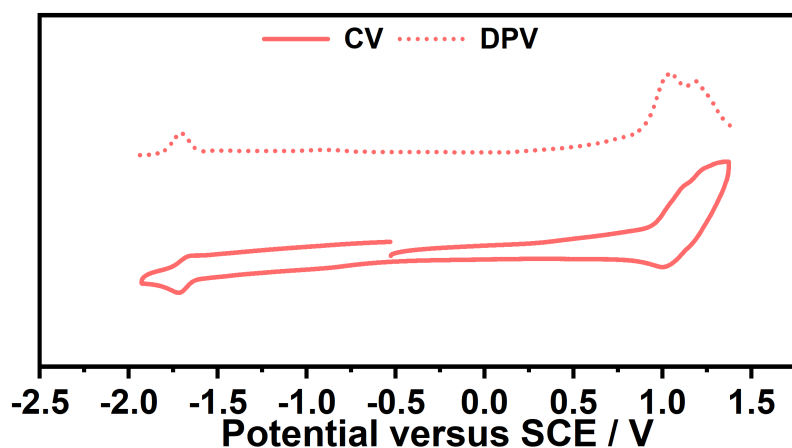


Figure S20. CV and DPV of 2,7-tBuCzNB in degassed MeCN with 0.1 M $[\text{tBu}_4\text{N}]\text{PF}_6$ as the supporting electrolyte and Fc/Fc^+ as the internal reference versus SCE (0.38 V vs. SCE).¹⁹ CV was performed at a sweep rate of 100 mV s^{-1} . DPV was conducted with an increment potential of 0.01 V and a pulse amplitude, width, and period of 50 mV, 0.06, and 0.5 s, respectively.

Table S3. Electrochemical data of **2,7-tBuCzNB**.^a

	E_{ox} / V	$E_{\text{red}} / \text{V}$	HOMO/ eV	LUMO/ eV	$\Delta E / \text{eV}$
2,7-tBuCzNB	0.66, 0.80	-2.09	-5.46	-2.71	2.75

^a In degassed MeCN with 0.1 M [ⁿBu₄N]PF₆ as the supporting electrolyte and Fc/Fc⁺ as the internal reference (0.38 V vs. SCE).¹⁹ The HOMO and LUMO energies were determined using the relation HOMO/LUMO = $-(E_{\text{ox}} / E_{\text{red}} + 4.8)$ eV,²¹ where E_{ox} and E_{red} are the peak of anodic and cathodic potentials from DPV relative to Fc/Fc⁺. ΔE is the energy gap between HOMO and LUMO.

Table S4. Φ_{PL} values of **2,7-tBuCzNB** in mCP films ($\lambda_{\text{exc}} = 440 \text{ nm}$).^a

	1 wt%	5 wt%	10 wt%	20 wt%	50 wt%
2,7-tBuCzNB	80 (78)	81 (72)	77 (70)	61 (54)	36 (31)

^a Φ_{PL} in nitrogen (Φ_{PL} in air).

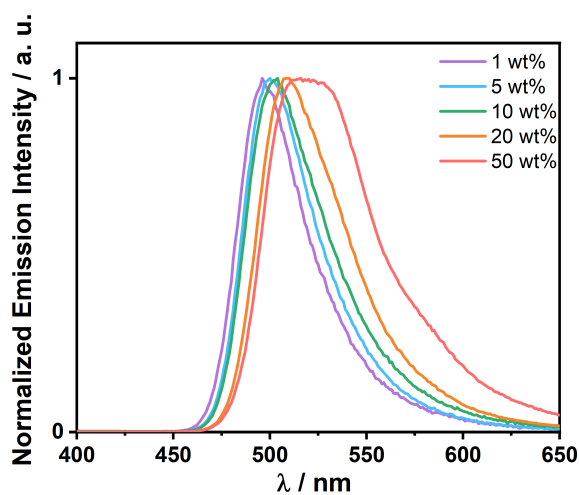


Figure S21. Steady-state PL spectra at 300 K of **2,7-tBuCzNB** films in mCP at different doping concentrations ($\lambda_{\text{exc}} = 340 \text{ nm}$).

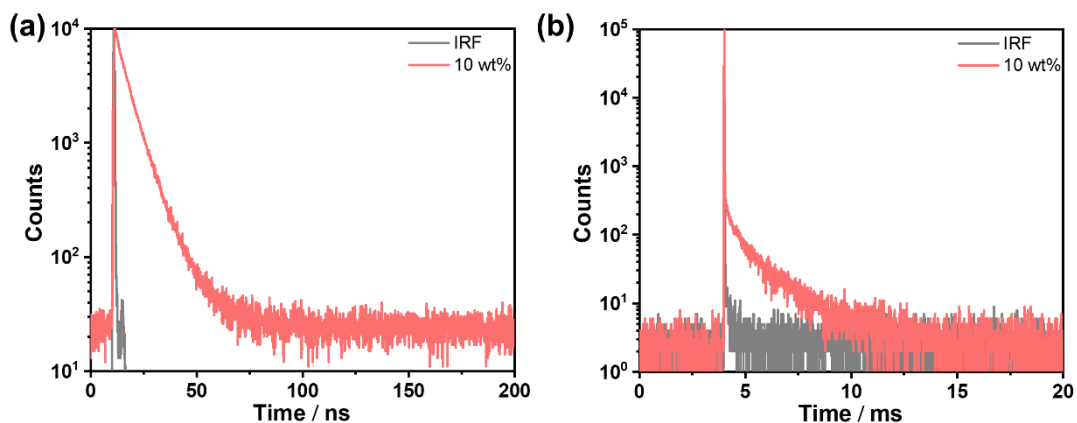


Figure S22. Time-resolved PL decays of 10 wt% doped film of **2,7-tBuCzNB** in mCP ($\lambda_{\text{exc}} = 375$ nm).

The kinetics parameters were calculated according to the following equations and summarized in Table S5.^{35, 36}

$$\Phi_{PL} = \Phi_p + \Phi_d \quad (\text{S1})$$

$$k_p = \frac{1}{\tau_p} \quad (\text{S2})$$

$$k_d = \frac{1}{\tau_d} \quad (\text{S3})$$

$$k_r^S = k_p \Phi_p \quad (\text{S4})$$

$$k_{ISC} = k_p (1 - \Phi_p) \quad (\text{S5})$$

$$k_{RISC} = \frac{k_p k_d \Phi_d}{k_{ISC} \Phi_p} \quad (\text{S6})$$

Where the Φ_p and Φ_d are the prompt fluorescent and delayed photoluminescence quantum yields, which are calculated by integrating the transient PL decays; k_p is the rate constant of prompt fluorescence; k_d is the rate constant of delayed fluorescence; k_r^S is the radiative decay rate constant of S_1 ; k_{ISC} is the intersystem crossing rate constant; k_{RISC} is the reverse intersystem crossing rate constant.

Table S5. Summary of kinetics parameters of 5 wt% **2,7-tBuCzNB** doped film in mCP.

	Φ_p / %	Φ_d / %	k_p / 10^8 s^{-1}	k_d / 10^2 s^{-1}	k_r^S / 10^7 s^{-1}	k_{ISC} / 10^7 s^{-1}	k_{RISC} / 10^2 s^{-1}
2,7-tBuCzNB	66	15	1.3	8.0	8.6	4.5	5.4

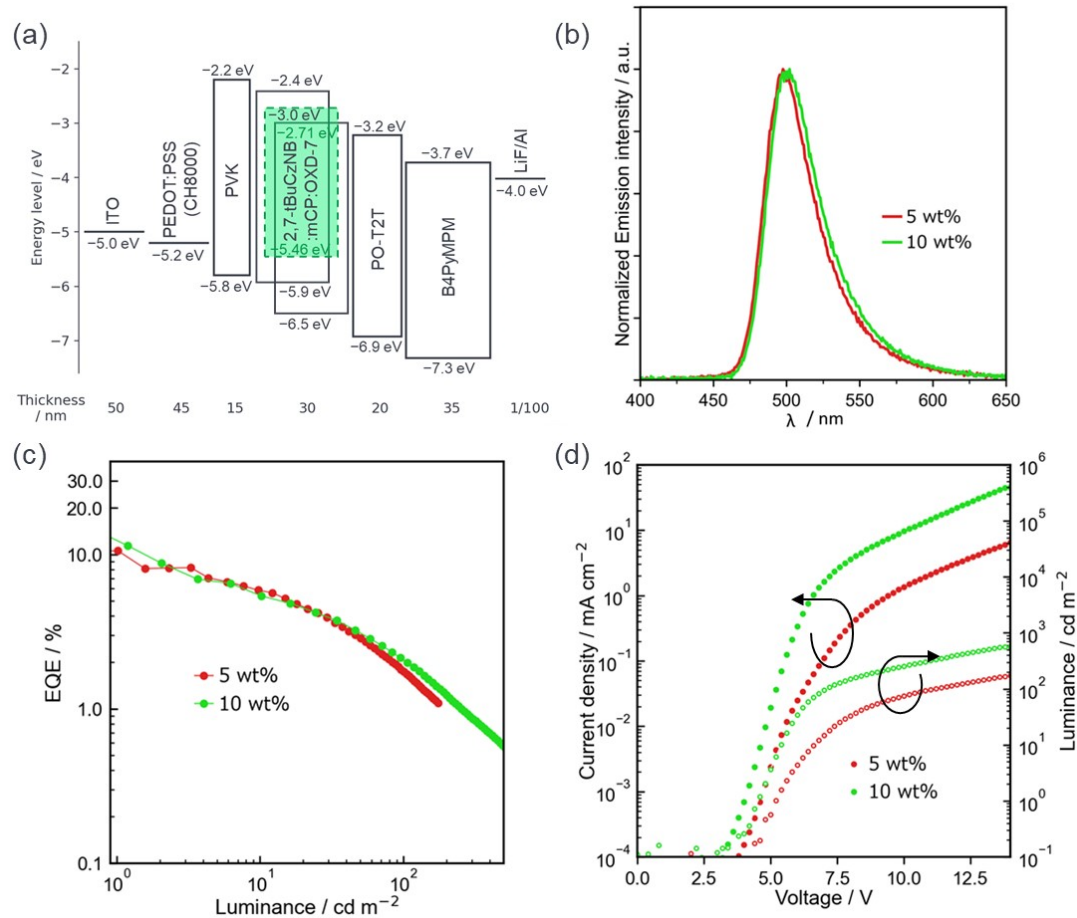


Figure S23. (a) Device structure, (b) electroluminescence spectra, (c) EQE–luminance curves, (d) current density–voltage–luminance characteristics of SP-OLEDs using 5 or 10 wt% **2,7-tBuCzNB**:mCP:30 wt% OXD-7 as the emitting layer.

Table S6. Φ_{PL} and device performances of **2,7-tBuCzNB** in mCP:OXD-7.

Doped concentration	Φ_{PL}^a / %	$\text{EQE}_{\text{max}}/\text{EQE}_{100}^b$ / %	V_{on}^c / V	λ_{EL} (FWHM) ^d / nm	CIE ^e (x, y)
5 wt%	81	10.6/1.7	5.2	498 (41)	(0.16, 0.53)
10 wt%	80	11.4/2.0	4.6	502 (43)	(0.17, 0.57)

^aMeasured in doped film in mCP; ^b maximum EQE and EQE at 100 cd m⁻², ^cturn on voltage at 1 cd m⁻², ^d EL peak wavelength and FWHM and ^eCIE coordinates at 1 mA cm⁻² in **2,7-tBuCzNB**:mCP:OXD-7.

References:

1. M. J. Frisch, G. W. Trucks, H. B. Schlegel, G. E. Scuseria, M. A. Robb, J. R. Cheeseman, G. Scalmani, V. Barone, G. A. Petersson, H. Nakatsuji, X. Li, M. Caricato, A. V. Marenich, J. Bloino, B. G. Janesko, R. Gomperts, B. Mennucci, H. P. Hratchian, J. V. Ortiz, A. F. Izmaylov, J. L. Sonnenberg, Williams, F. Ding, F. Lipparini, F. Egidi, J. Goings, B. Peng, A. Petrone, T. Henderson, D. Ranasinghe, V. G. Zakrzewski, J. Gao, N. Rega, G. Zheng, W. Liang, M. Hada, M. Ehara, K. Toyota, R. Fukuda, J. Hasegawa, M. Ishida, T. Nakajima, Y. Honda, O. Kitao, H. Nakai, T. Vreven, K. Throssell, J. A. Montgomery Jr., J. E. Peralta, F. Ogliaro, M. J. Bearpark, J. J. Heyd, E. N. Brothers, K. N. Kudin, V. N. Staroverov, T. A. Keith, R. Kobayashi, J. Normand, K. Raghavachari, A. P. Rendell, J. C. Burant, S. S. Iyengar, J. Tomasi, M. Cossi, J. M. Millam, M. Klene, C. Adamo, R. Cammi, J. W. Ochterski, R. L. Martin, K. Morokuma, O. Farkas, J. B. Foresman, D. J. Fox, *Gaussian 16, Revision C. 01.*, Gaussian, Inc., Wallingford CT., 2016.
2. C. Adamo and V. Barone, Toward reliable density functional methods without adjustable parameters: The PBE0 model, *J. Chem. Phys.*, 1999, **110**, 6158-6170.
3. T. H. Dunning, Jr., Gaussian basis sets for use in correlated molecular calculations. I. The atoms boron through neon and hydrogen, *J. Chem. Phys.*, 1989, **90**, 1007-1023.

4. S. Grimme, Density functional calculations with configuration interaction for the excited states of molecules, *Chem. Phys. Lett.*, 1996, **259**, 128-137.
5. S. Hirata and M. Head-Gordon, Time-dependent density functional theory within the Tamm–Dancoff approximation, *Chem. Phys. Lett.*, 1999, **314**, 291-299.
6. R. Dennington, T. Keith and J. Millam, *GaussView, Version 6*, Semichem Inc., Shawnee Mission KS, 2019.
7. C. Hättig, Geometry optimizations with the coupled-cluster model CC2 using the resolution-of-the-identity approximation, *J. Chem. Phys.*, 2003, **118**, 7751-7761.
8. A. Hellweg, S. A. Grün and C. Hättig, Benchmarking the performance of spin-component scaled CC2 in ground and electronically excited states, *Phys. Chem. Chem. Phys.*, 2008, **10**, 4119-4127.
9. K. Momma and F. Izumi, VESTA 3 for three-dimensional visualization of crystal, volumetric and morphology data, *J. Appl. Crystallogr.*, 2011, **44**, 1272-1276.
10. O. S. Lee and E. Zysman-Colman, *Digichem (version 6) InSilico Computing*, St Andrews, Scotland, 2024.
11. O. Lee, M. Gather and E. Zysman-Colman, Digichem: Computational Chemistry For Everyone, *Digital Discovery*, 2024, **3**, 1695-1713.
12. N. M. O'Boyle, A. L. Tenderholt and K. M. Langner, Cclib: a library for package - independent computational chemistry algorithms, *J. Comput. Chem.*, 2008, **29**, 839-845.
13. W. Humphrey, A. Dalke and K. Schulten, VMD: visual molecular dynamics, *J. Mol. Graph. Model.*, 1996, **14**, 33-38.
14. J. E. Stone, *An efficient library for parallel ray tracing and animation*, 1998.
15. J. D. Hunter, Matplotlib: A 2D graphics environment, *Comput. Sci. Eng.*, 2007, **9**, 90-95.
16. N. M. O'Boyle, M. Banck, C. A. James, C. Morley, T. Vandermeersch and G. R. Hutchison, Open Babel: An open chemical toolbox, *J. Cheminformatics*, 2011, **3**, 1-14.
17. N. M. O'Boyle, C. Morley and G. R. Hutchison, Pybel: a Python wrapper for the OpenBabel cheminformatics toolkit, *Chem. Cent. J.*, 2008, **2**, 1-7.

18. X. Gao, S. Bai, D. Fazzi, T. Niehaus, M. Barbatti and W. Thiel, Evaluation of spin-orbit couplings with linear-response time-dependent density functional methods, *J. Chem. Theory Comput.*, 2017, **13**, 515-524.
19. V. V. Pavlishchuk and A. W. Addison, Conversion constants for redox potentials measured versus different reference electrodes in acetonitrile solutions at 25 C, *Inorg. Chim. Acta*, 2000, **298**, 97-102.
20. J. Pommerehne, H. Vestweber, W. Guss, R. F. Mahrt, H. Bässler, M. Porsch and J. Daub, Efficient two layer leds on a polymer blend basis, *Adv. Mater.*, 1995, **7**, 551-554.
21. C. M. Cardona, W. Li, A. E. Kaifer, D. Stockdale and G. C. Bazan, Electrochemical Considerations for Determining Absolute Frontier Orbital Energy Levels of Conjugated Polymers for Solar Cell Applications, *Adv. Mater.*, 2011, **23**, 2367-2371.
22. G. A. Crosby and J. N. Demas, Measurement of photoluminescence quantum yields. Review, *J. Phys. Chem.*, 1971, **75**, 991-1024.
23. W. H. Melhuish, Quantum efficiencies of fluorescence of organic substances: effect of solvent and concentration of the fluorescent solute1, *J. Phys. Chem.*, 1961, **65**, 229-235.
24. N. Greenham, I. Samuel, G. Hayes, R. Phillips, Y. Kessener, S. Moratti, A. Holmes and R. Friend, Measurement of absolute photoluminescence quantum efficiencies in conjugated polymers, *Chem. Phys. Lett.*, 1995, **241**, 89-96.
25. N. T. Johnson, P. G. Waddell, W. Clegg and M. R. Probert, Remote Access Revolution: Chemical Crystallographers Enter a New Era at Diamond Light Source Beamline I19, *Crystals*, 2017, **7**, 360.
26. D. Allan, H. Nowell, S. Barnett, M. Warren, A. Wilcox, J. Christensen, L. Saunders, A. Peach, M. Hooper and L. Zaja, A Novel Dual Air-Bearing Fixed- χ Diffractometer for Small-Molecule Single-Crystal X-ray Diffraction on Beamline I19 at Diamond Light Source, *Crystals*, 2017, **7**, 336.
27. *APEX3*, Bruker AXS Inc., Madison (WI), USA, 2018.
28. *SAINT v8.40.*, Bruker AXS Inc., Madison (WI), USA, 2019.
29. G. M. Sheldrick, *TWINABS 2012/1.*, Bruker AXS Inc., Madison (WI), USA, 2012.

30. G. M. Sheldrick, A short history of SHELX, *Acta Crystallogr., Sect. A: Found. Crystallogr.*, 2008, **64**, 112-122.
31. G. M. Sheldrick, Crystal structure refinement with SHELXL, *Acta Crystallogr., Sect. C: Struct. Chem.*, 2015, **71**, 3-8.
32. A. L. Spek, PLATON SQUEEZE: a tool for the calculation of the disordered solvent contribution to the calculated structure factors, *Acta Crystallogr., Sect. C: Struct. Chem.*, 2015, **71**, 9-18.
33. A. L. Spek, Structure validation in chemical crystallography, *Acta Crystallogr., Sect. D: Biol. Crystallogr.*, 2009, **65**, 148-155.
34. O. V. Dolomanov, L. J. Bourhis, R. J. Gildea, J. A. Howard and H. Puschmann, OLEX2: a complete structure solution, refinement and analysis program, *J. Appl. Crystallogr.*, 2009, **42**, 339-341.
35. K. Masui, H. Nakanotani and C. Adachi, Analysis of exciton annihilation in high-efficiency sky-blue organic light-emitting diodes with thermally activated delayed fluorescence, *Org. Electron.*, 2013, **14**, 2721-2726.
36. Y. Tsuchiya, S. Diesing, F. Bencheikh, Y. Wada, P. L. Dos Santos, H. Kaji, E. Zysman-Colman, I. D. W. Samuel and C. Adachi, Exact Solution of Kinetic Analysis for Thermally Activated Delayed Fluorescence Materials, *J. Phys. Chem. A*, 2021, **125**, 8074-8089.